Optimum Design of Coplanar Waveguide for $LiNbO_3$ Optical Modulator

Xiang Zhang and Tanroku Miyoshi, *Member, IEEE*

Abstract— **In this paper, we first present a novel finite element method combined with the conformal mapping (FEM-CM) for a quasi-static analysis of coplanar waveguides (CPW). Using this approach, the optimum CPW structures for the use in the Ti:$LiNbO_3$ optical modulator are discussed in detail to realize optical-microwave phase velocity match and electrode-source characteristic impedance match. Our numerical results reveal that both conditions can be satisfied simultaneously by introducing a SiO_2 buffer layer and thicker electrodes. The modulator efficiency with respect to the voltage-length product is also evaluated for the optimized structures. Finally, the design guidelines to the optimum CPW structure are presented.**

I. Introduction

A MACH-ZEHNDER Ti:$LiNbO_3$ optical modulator is a promising component for high speed and broad-band optical communication systems. A coplanar waveguide (CPW) has often been used as a traveling-wave electrode in such a modulator [1]–[5]. Furthermore, for the broadband operation of the modulator, a thick-plated electrode (typically $\geq$ 10 μm) and a relatively thick SiO_2 buffer layer (typically $\geq$ 1.0 μm) have been introduced to the CPW [3]–[10]. Both the thick-plated electrode and the thick buffer layer contribute to the decrease of microwave effective index, but the use of thick buffer layer results in the increase of driving voltage because the spatial overlap of optical and microwave field decreases. Therefore, it has been pointed out [10] that there is a tradeoff between the modulation bandwidth Δf and the driving half-wavelength voltage V_π.

So far, as a figure of merit of traveling-wave electrode modulators, the bandwidth-voltage ratio $\Delta f/V_\pi$ has been evaluated. However, in the optical modulator with CPW electrodes, as shown in Fig. 1, the voltage V_π is mainly determined by the buffer layer thickness. Therefore, once the buffer layer thickness is given, the figure of merit of the CPW modulator depends primarily on the phase velocity match between microwave and optical wave. Further, in the above figure of merit, the electrode impedance matching to a 50-Ω source is not considered for the efficient utilization of the microwave voltage. Although many papers have been reported on the design of $LiNbO_3$ optical modulators [11]–[16], the optimum structure of the modulator, which realizes the velocity match and the impedance match simultaneously, has not been discussed completely. All of the authors exerted themselves on the behalf of velocity match, but neglected the very important impedance match. Therefore, in this paper, taking the above background into consideration, we will search first the optimum structures satisfying both the velocity match and the impedance match for a practical thickness of buffer layer and then evaluate the driving voltage V_π using a series set of optimum parameters discovered.

Manuscript received July 29, 1993; revised June 27, 1994.

The authors are with the Department of Electrical and Electronics Engineering, Kobe University, Kobe 657, Japan.

IEEE Log Number 940761.

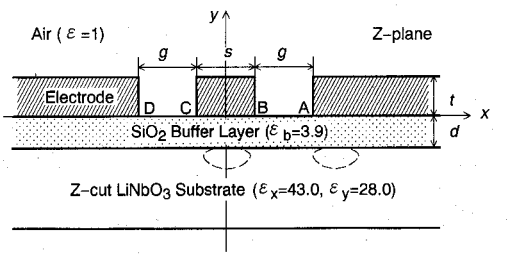

Fig. 1. Coplanar waveguide optical modulator model.

In this paper, a quasi-static analysis is presented for the analysis of the CPW electrode based on the finite element method (FEM). In general, the FEM is very well-suited to the problem within limited regions defined by closed boundaries, but when the boundary is not closed, as in the case of CPW, we have to develop a technique dealing with open region. Although we have proposed various methods for modeling large empty open spaces satisfactorily [17], [18], they are not directly applicable to the present problem because the external open region is not homogeneous. Thus, we propose a novel FEM combined with conformal mapping (FEM-CM) in this paper. The basic technique of the method is to map the CPW cross-section extending laterally in open space into the closed region by using a conformal mapping transformation first, and then the static capacitance of the reduced model space is analyzed by the FEM. This is due to the fact that the static energy of the system is preserved after the mapping.

After the validity of the method is verified by comparing results with those calculated by the spectral domain method [12], the optimum coplanar waveguide structures are discussed in detail to realize the microwave effective index of 2.15 (we assume the effective index for optical TM mode is close to 2.15 in a Z-cut $LiNbO_3$ substrate) and the characteristic impedance of 50 Ω. Further, we study the cross-sectional overlap integral [11] between the guided optical power and the microwave field using a series set of optimum parameters discovered in this paper. Our numerical results reveal that both the phase velocity match and the impedance match can be achieved simultaneously for a series set of structures, and that the voltage-length product changes slightly for such optimized structures if the thickness of buffer layer is fixed. Finally, the design guidelines to the optimum CPW structure are summarized.

II. FEM Combined with Conformal Mapping

The cross-sectional configuration of the $LiNbO_3$ Mach-Zehnder optical modulator with a CPW electrode is shown in Fig. 1. The CPW electrodes of thickness t lie on the top of SiO_2 buffer layer of thickness d, which is deposited on the Z-cut $LiNbO_3$ substrate. The width of center electrode is s, while the width of gap between the center electrode and a ground electrode is g. The $LiNbO_3$ substrate is assumed to be thick enough. The anisotropic dielectric constant of the Z-cut $LiNbO_3$ are 43 and 28 in the x and y directions, respectively, and the dielectric constant of the SiO_2 buffer layer is 3.9.

Although a relatively thin $LiNbO_3$ substrate is used to eliminate the first higher-order mode (radiation mode) practically, the thickness of the substrate is assumed to be infinite in this analysis, because the CPW characteristics hardly change with the thickness of the substrate when it is greater than 200 μm [19]. Further, it is known that the dispersion effect of the dominant mode is negligibly small up to the frequency when the dominant mode begins to couple to the first higher order mode, typically 40 GHz for a 200-μm-thick substrate [5].

Because the dimension of the CPW is very small compared to the microwave effective wavelength of our interest, a quasi-TEM approximation gives reasonable results. In the quasi-static approximation, the static potential $\phi(x, y)$ is governed by the following Laplace's equation

$$\varepsilon_x \frac{\partial^2 \phi(x,y)}{\partial x^2} + \varepsilon_y \frac{\partial^2 \phi(x,y)}{\partial y^2} = 0, \tag{1}$$

where $\varepsilon_x = \varepsilon_y = 1.0\ (y>0)$, $\varepsilon_x = \varepsilon_y = \varepsilon_b = 3.9\ (-d<y<0)$, and $\varepsilon_x = 43$, $\varepsilon_y = 28$ $(y<-d)$. Using the coordinate transformation $y' = (\varepsilon_x/\varepsilon_y)1/2y$, (1) is rewritten simply as

$$\frac{\partial^2 \phi(x,y')}{\partial x^2} + \frac{\partial^2 \phi(x,y')}{\partial y'^2} = 0. \tag{2}$$

As the first step to solve (2), the upper half plane $(y>0)$ in Fig. 1, which consists of the thick electrodes and the covered air, and the lower half plane $(y<0)$, which contains the buffer layer and the substrate, are mapped separately into the closed region in W-plane as shown in Fig. 2. Here, the following transformation function is used for conformal mapping

$$w = \int_b^z \left(\frac{dw}{dz}\right) dz = \int_1^{z/b} \frac{1 + b/a}{(1-\zeta^2)^{1/2}(1 - b^2\zeta^2/a^2)^{1/2}} d\zeta, \tag{3}$$

where $a(= s/2 + g)$ and $b(= s/2)$ are the coordinates of A and B in Z-plane, respectively, and $\zeta = z/b$, $z = x + jy'$, $w = u + jv$. Under such a transformation, A, B, C, D in the Z-plane are mapped into the W-plane as

$$A = j2K(k'), B = 0, C = 2K(k), D = 2K(k) + j2K(k'). \tag{4}$$

where $K(k)$ denotes the complete elliptic integral of first kind. The modulus k is given by $k = 2\sqrt{ab}/(a+b)$ and $k' = \sqrt{1-k^2}$.

In order to map the contour of the electrodes and the interface between the buffer layer and the substrate into W-plane, the transformation function (3) is rewritten, using $\zeta = \sin\gamma$, as

$$w = \int_{1/2}^{\theta} \frac{1 + b/a}{(1 - b^2\sin^2\gamma/a^2)^{1/2}} d\gamma = \left(1 + \frac{b}{a}\right)\{F(\theta|m) - K(m)\}, \tag{5}$$

where $m = b/a$, $\theta = \sin^{-1}\zeta$ and $F(\theta|m)$ denotes the elliptic integral of first kind.

Next, to calculate $F(\theta|m)$ numerically, θ is replaced by

$$\theta = \phi + j\psi. \tag{6}$$

Then, $F(\theta|m)$ is resolved into real and imaginary parts as [20]

$$w = \left(1 + \frac{b}{a}\right)\{F(\alpha|m) - K(m) + jF(\beta|m')\}, \tag{7}$$

where $m' = \sqrt{1-m^2}$. When the coordinates ϕ and ψ in Z-plane are given, α and β in (7) are determined as follows.

$\cot^2\alpha$ is given by the positive solution of the quadratic equation

$$\chi^2 - (\cot^2\phi + m^2\sinh^2\psi\,\csc^2\phi - m'^2)\chi - m'^2\cot^2\phi = 0, \tag{8}$$

and β is derived from the relation

$$m^2\tan^2\beta = \tan^2\phi\cot^2\alpha - 1. \tag{9}$$

Thus, the contour of the electrodes and the interface between the buffer layer and the substrate in Z-plane are mapped into W-plane as shown in Fig. 2. In the Fig. 2(a) and (b), the

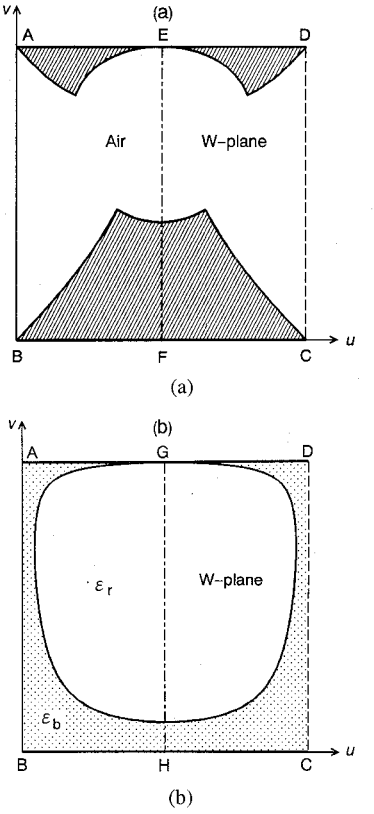

Fig. 2 Mapping into W-plane of (a) upper half space and (b) lower half space.

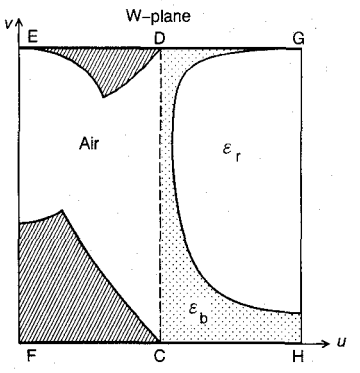

Fig. 3. Mapped model used in FEM analysis.

potential and the electric field distribution along the interface AB and CD between SiO_2 and air are identical because they are transformed by the same mapping function. Further, since Fig. 2(a) and (b) is symmetric with respect to the center lines EF and GH, respectively, only the reduced region shown in Fig. 3 is analyzed by the FEM, where the contours EF and GH are magnetic wall boundaries.

The basic equation for the FEM analysis in W-plane is given by

$$\nabla \cdot \varepsilon(u,v)\nabla\phi(u,v) = 0, \tag{10}$$

where $\varepsilon(u,v) = \varepsilon_r = \sqrt{\varepsilon_x \varepsilon_y}$ in $LiNbO_3$, $\varepsilon(u,v) = \varepsilon_b$ in SiO_2, and $\varepsilon(u,v) = 1.0$ in air, respectively. Using the energy functional, which is the variational representation of (10), the FEM solution and then the static capacitance C per unit length of the CPW is obtained numerically. The effective index N_{eff} and the characteristic impedance Z_c of the CPW are given by

$$N_{eff} = \sqrt{C/C_0}, \tag{11}$$

$$Z_c = \frac{1}{v_0\sqrt{CC_0}}, \tag{12}$$

where C_0 denotes the capacitance per unit length of the CPW when both SiO_2 and $LiNbO_3$ are replaced with air. v_0 is the velocity of light in free space.

The method proposed here is general and applicable to most of planar transmission lines with arbitrary electrode cross-section. Please recall that the spectral domain method, which is an established powerful tool in the analysis of planar transmission lines, is applicable only to thick electrodes with the rectangular cross-sectional shape even if it is extended [12]. In addition, compared with the conventional FEM analysis where an imaginary mathematical boundary has to be assumed, the required number of nodes used in the FEM-CM analysis is drastically reduced.

As for the analysis of asymmetric structures such as an asymmetric CPW with different width of the outside ground electrodes, the FEM-CM method is still applicable provided the potential distribution along the interface between the upper and lower spaces is matched in W-plane each other. Of course, for such an asymmetric structure, the mapped upper and lower space in W-plane cannot be reduced to one closed region any more. Incidentally, such an asymmetric electrode of the CPW will not be preferable to the broad-band operation because the leakage mode in the substrate will be excited at a lower frequency.

III. Overlap Integral and Voltage-Length Product

When the phase velocity match and the impedance match are achieved, the modulation bandwidth becomes infinite if the microwave transmission loss is ignored. As shown later, we will find a series set of CPW structures that satisfy both the velocity match and the impedance match when the buffer layer thickness is given. For such a series set of structures, we will further evaluate the modulation efficiency with respect to the product of the driving voltage and the modulator length.In general, the change in the propagation constant $\Delta\beta_i$ ($i = 1, 2$) of a guided mode in each channel waveguide due to the change in the extraordinary refractive index in response to an externally applied field along the y axis is given by

$$\Delta\beta_i + \frac{\pi}{\lambda_0} n_e^3 r_{33} \Gamma_i \frac{V}{g}, \tag{13}$$

where λ_0 is the optical wavelength in free space, $n_e = 2.15$ the extraordinary refractive index of $LiNbO_3$ substrate, $r_{33} = 30.8 \times 10^{-12}$ m/V the electrooptic coefficient, V the applied voltage, and g the gap between the electrodes. Γ_i ($i = 1, 2$) is the overlap integral factor for each channel waveguide defined by

$$\Gamma_i = \frac{g}{V} \frac{\int\int E_{op}^2(x,y) E_y(x,y) dxdy}{\int\int E_{op}^2(x,y) dxdy}, \tag{14}$$

where $E_{op}^2(x,y)$ is the optical power distribution and $E_y(x,y)$ is the y component of the microwave electric field.

When we approximate the fundamental TM mode profile in the weekly guiding optical waveguide beneath the buffer layer by Gaussian function in the lateral direction and Hermite-Gaussian function in the depth direction, the normalized $E_{op}^2(x,y)$ is given by

$$E_{op}^2(x,y) = \frac{4(y+d)^2}{w_x w_y^3 \pi} \exp\left\{-\left(\frac{x-p}{w_x}\right)^2\right\} \cdot \exp\left\{-\left(\frac{y+d}{w_y}\right)^2\right\}, \tag{15}$$

where w_x and w_y are the mode spot radius in the x and y direction, respectively, p denotes the center position of optical waveguide, and $y < 0$.

On the other hand, the microwave electric field $E(x,y)$ in Z-plane is obtained from the W-plane static potential $\phi(u,v)$ by

$$E_x(x,y) = -\left\{\frac{\partial\phi(u,v)}{\partial u} Re\left(\frac{dw}{dz}\right) + \frac{\partial\phi(u,v)}{\partial v} Im\left(\frac{dw}{dz}\right)\right\}, \tag{16}$$

$$E_y(x,y) = \left(\frac{\varepsilon_x}{\varepsilon_y}\right)^{1/2} \left\{\frac{\partial\phi(u,v)}{\partial u} Im\left(\frac{dw}{dz}\right) - \frac{\partial\phi(u,v)}{\partial v} Re\left(\frac{dw}{dz}\right)\right\}. \tag{17}$$

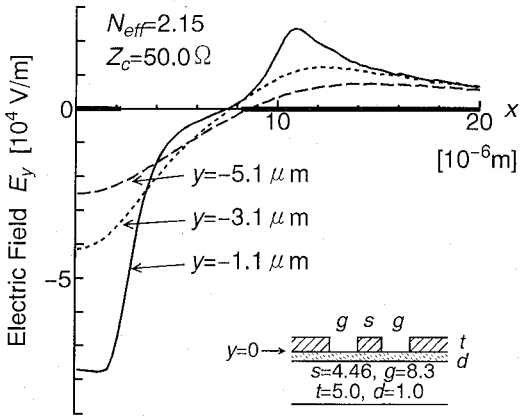

Fig. 4. E_y distribution along x at various y coordinates in the Z-plane.

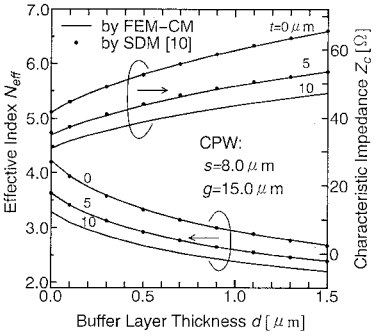

Fig. 5. Comparison between the FEM-CM and the spectral domain method (SDM) [10]: Influence of the buffer layer thickness and the electrode thickness on N_{eff} and Z_c. $s = 8$ μm and $g = 15$ μm.

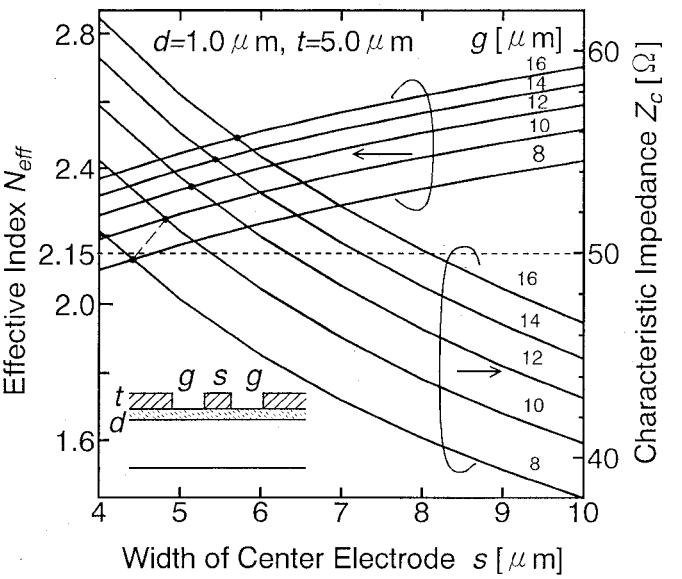

Fig. 6. Search for the optimum electrode width s and the gap width g to realize both $N_{eff} = 2.15$ and $Z_c = 50\Omega$ when $d = 1.0$ μm and $t = 5$ μm.

As an example, the computed E_y distributions along the x direction at various y coordinates in $LiNbO_3$ are shown in Fig. 4. It is found from Fig. 4 that the electric fields E_y are quite different in the two optical waveguides. The electric field beneath the center conductor is much larger than that under the ground conductor. Thus, in case of the CPW electrode, the overlap integral factors $|\Gamma_1|$ and $|\Gamma_2|$ must be evaluated separately. Note that the peak of the electric field E_y under central electrode is not necessarily at the center due to the electrode tip effects.

When we consider the push-pull electrooptic effect of a Mach-Zehnder type modulator, the half-wave voltage V_π defined by $(|\Delta\beta_1|+|\Delta\beta_2|)L = \pi$ is a proper index evaluating the modulation efficiency, which is represented, using (13), as

$$V_\pi \cdot L = \frac{\lambda_0}{\pi n_e^3 r_{33}(|\Gamma_1| + |\Gamma_2|)/g}, \tag{18}$$

where L denotes the modulator length.

IV. Optimization of CPW Structure

To verify the validity of the technique presented in this paper, the characteristics of the CPW are calculated first as a function of the thickness of buffer layer as shown in Fig. 5 and compared with the results by the spectral domain method (SDM) [12]. Fig. 5 reveals that the FEM-CM is applicable in the analysis of the CPW with almost the same accuracy as for SDM. It is found from Fig. 5 that a combination of thick buffer layer and thick electrode can effectively control the characteristics of the modulator. A thick electrode can lower both the microwave effective index and the device impedance. On the other hand, a thick buffer layer can compensate the impedance decrease and further lower the microwave effective index. However, as shown later, it will deteriorate the overlap between the microwave and the optical field and accordingly make worse the efficiency of the modulator. In the following optimization procedure, the thickness of buffer layer d is set to be 1.0 and 1.2 μm.

In Fig. 6, the optimum center electrode width s and gap width g are searched to realize both $N_{eff} = 2.15$ and $Z_c = 50\ \Omega$ simultaneously, when the thickness of electrode t and the buffer layer d are fixed to be 5 and 1.0 μm, respectively. Fig. 6 shows that increasing gap width enlarges both the effective index and the characteristic impedance, and that increasing center electrode width lowers the characteristic impedance but makes the effective index larger. Compared with Fig. 5, it is found that the electrode thickness and the gap width play an inverse role in the performance. So do the center electrode width and buffer layer thickness. It is found from Fig. 6 that both $N_{eff} = 215$ and $Z_c = 50\ \Omega$ are realized simultaneously when $s = 4.46$ μm and $g = 8.3$ μm.

Such an optimization procedure is repeated for various values of electrode and buffer layer thickness. The optimized series set of the CPW geometrical parameters are summarized in Fig. 7. It is shown that for a certain buffer layer thickness, the optimum width of gap g increases with the electrode thickness t while the width of the center electrode s hardly changes. That means that the optimum gap width g and the electrode thickness t compensate for each other, while the buffer layer thickness d and the center electrode width s compensate for each other.

In the above optimization procedure, only the phase velocity match and the impedance match are evaluated. To design

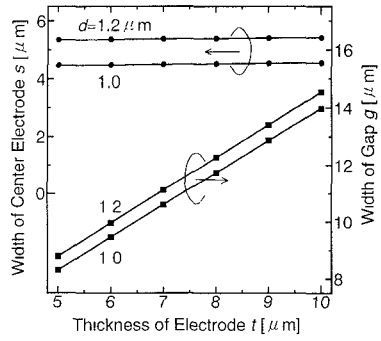

Fig. 7. Optimized structures of the CPW to realize both $N_{eff} = 2.15$ and $Z_c = 50\ \Omega$.

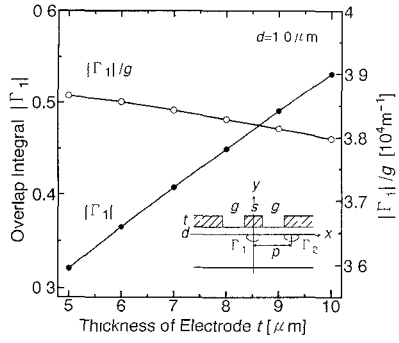

Fig. 8. Overlap integral $|\Gamma_1|$ as a function of electrode thickness for the optimized structures shown in Fig. 7. $d = 1.0\ \mu$m.

an efficient optical modulator, we should further study the voltage-length product mentioned in Section III using the series set of optimum parameters shown in Fig. 7.

Fig. 8 shows the calculated overlap integral $|\Gamma_1|$ of the optical waveguide under the center electrode for the optimized structures shown in Fig. 7, where the thickness of buffer layer is $d = 1.0\ \mu$m, and the optical mode radius is set to be $w_x = 2.0\ \mu$m, $w_y = 2.0\ \mu$m and $\lambda_0 = 1.3\ \mu$m. Fig. 8 shows that the overlap integral $|\Gamma_1|$ increases with the thickness of electrode t from 5 μm to 10 μm, but the value of $|\Gamma_1|/g$ decreases only 2%. This is because when d is fixed, the optimum s hardly changes with t as mentioned before, and then the electric field under center electrode is kept almost constant. Next, the overlap integral $|\Gamma_2|$ concerning the ground electrode is calculated as shown in Fig. 9 as a function of the optical waveguide center position for the optimized structures shown in Fig. 7. It is found from Fig. 9 that there is an optimum waveguide position that makes $|\Gamma_2|$ maximum. It is located approximately 2 μm, which is nearly equal to the mode spot radius, outside from the inner edge of the ground electrode. Here, please note that $|\Gamma_1|$ is much larger than the maximum value of $|\Gamma_2|$. This is due to the fact that the electric field under center electrode is much stronger than that of other place as shown in Fig. 4.

Finally, using the calculated $|\Gamma_1|$ and $|\Gamma_2|$ for various optical mode spot radii, the product $V_\pi \cdot L$ for the optimized structures shown in Fig. 7 is evaluated as shown in Fig. 10. It is found that the product $V_\pi \cdot L$ increases slowly with electrode thickness t for a fixed buffer layer. This is because $V_\pi \cdot L$ mainly depends on $|\Gamma_1|/g$, which does not change so much with t as shown in

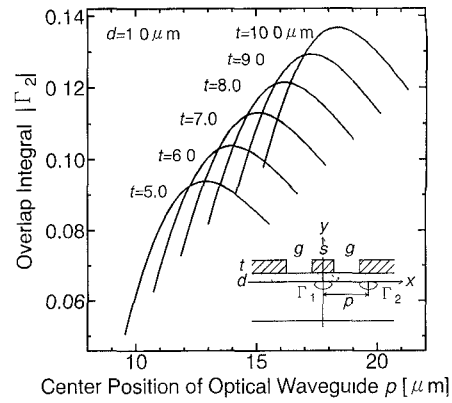

Fig. 9. Overlap integral $|\Gamma_2|$ as a function of optical waveguide center position p for the optimized structures shown in Fig. 7. $d = 1.0\ \mu$m.

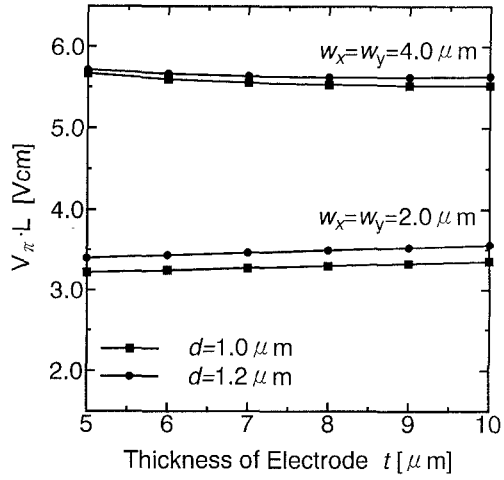

Fig. 10. $V_\pi \cdot L$ product for the optimized structures shown in Fig. 7 and for $w_x = w_y = 2\ \mu$m and $w_x = w_y = 4\ \mu$m.

Fig. 8. It may be said from Fig. 10 that when the thickness of the buffer layer is fixed, making the electrode thicker will not only deteriorate the modulation efficiency seriously or eliminate the evanescent coupling between the two optical waveguides effectively because larger gap width is available in this situation, but it will also lower the microwave losses. We encourage the practical device designer to employ a thicker electrode when taking into consideration the evanescent coupling between optical waveguide and microwave losses.

In addition, since it is also found from Fig. 10 that the smaller the optical mode spot size, the smaller the $V_\pi \cdot L$ product as was pointed out in [21], a narrow channel waveguide with large relative refractive index change is preferable for an efficient modulator unless the small spot size will suffer a coupling loss to single mode fibers.

From the above discussion, the design guideline to the optimum CPW Ti:LiNbO$_3$ optical modulator is summarized as follows:

1) Design an optical waveguide with a smaller mode spot size.
2) Choose the width of center electrode and then the thickness of buffer layer according to Fig. 7.

3) Choose the width of gap and then the thickness of electrode according to Fig. 7, taking into consideration the evanescent coupling between the two optical waveguides and the microwave loss.

V. Conclusion

A novel FEM combined with the conformal mapping has been presented to analyze the CPW for the use of the Ti:$LiNbO_3$ optical modulator. A large open space of the CPW is mapped satisfactorily into the closed region by a conformal mapping for the accurate FEM analysis. The concept of the method proposed is general and applicable to most of planar transmission lines with arbitrary conductor cross-section. In the CPW design, a series set of the optimum CPW geometrical parameters are found to realize the microwave effective index of 2.15 and the characteristic impedance of 50 Ω for the practical buffer layer thickness of 1.0 and 1.2 μm. The voltage-length product is found to change slightly for the optimized CPW structures when the thickness of buffer layer is fixed. The design guidelines to the optimum CPW structure are also presented. In this paper, the microwave loss of the CPW electrode and the evanescent coupling between the optical waveguides are not evaluated quantitatively, which will be presented elsewhere.

References

[1] R. A. Becker, "Traveling-wave electro-optic modulator with maximum bandwidth-length product," *Appl. Phys. Lett.*, vol. 45, no. 11, pp. 1168–1170, Dec. 1984.

[2] D. W. Dolfi and M. Nazarathy, "40GHz electro-optic modulator with 7.5V drive voltage," *Electron. Lett.*, vol. 24, no. 9, pp. 528–529, Apr. 1988.

[3] M. Rangaraj, T. Hosoi, and M. Kondo, "A wide-band Ti:$LiNbO_3$ optical modulator with a conventional coplanar waveguide type electrode," *IEEE Photon. Technol. Lett.*, vol. 4, no. 9, pp. 1020–1022, Sept. 1992.

[4] D. W. Dolfi and T. R. Ranganath, "50GHz velocity-matched broad wavelength $LiNbO_3$ modulator with multimode active section," *Electron. Lett.*, vol. 28, no. 13, pp. 1197–1198, June 1992.

[5] G. K. Gopalakrishnan, C. H. Bulmer, W. K. Burns, R. W. McElhanon, and A. S. Greenblatt, "40GHz, low half-wave voltage Ti:$LiNbO_3$ intensity modulator," *Electron. Lett.*, vol. 28, no. 9, pp. 826–827, Apr. 1992.

[6] M. Seino, N. Mekada, T. Namiki, and H. Nakajima, "33-GHz-cm broadband Ti:$LiNbO_3$ Mach-Zehnder modulator," *Tech. Dig. ECOC'89, Gothenburg*, paper ThB22-5, 1989.

[7] M. Seino, N. Mekada, Y. Kubota, M. Doi, and T. Nakazawa, "20GHz 3dB-bandwidth Ti:$LiNbO_3$ Mach-Zehnder modulator," *Tech. Dig. ECOC'90, Amsterdam*, postdeadline paper ThG1.4, 1990.

[8] H. Miyamoto, H. Ohta, K. Tabuse, H. Iwaoka, and Y. Miyagawa, "A broad-band traveling-wave Ti:$LiNbO_3$ optical phase modulator," *J. Appl. Phys.*, vol. 30, no. 3A, pp. L383–L385, Mar. 1991.

[9] K. Kawano, T. Kitoh, H. Jumonji, T. Nozawa, and M. Yanagibashi, "New traveling-wave electrode Mach-Zehnder optical modulator with 20GHz bandwidth and 4.7V driving voltage at 1.52 μm wavelength," *Electron. Lett.*, vol. 25, no. 20, pp. 1382–1383, Sept. 1989.

[10] K. Noguchi, O. Mitomi, K. Kawano, and M. Yanagibashi, "Highly Efficient 40-GHz bandwidth Ti:$LiNbO_3$ optical modulator employing ridge structure," *IEEE Photon. Technol. Lett.*, vol. 5, no. 1, pp. 52–54, Jan. 1993.

[11] C. M. Kim and R. V. Ramaswamy, "Overlap integral factors in integrated optic modulators and switches," *J. Lightwave Technol.*, vol. 7, no. 7, pp. 1063–1070, July 1989.

[12] T. Kitazawa, D. Polifko, and H. Ogawa, "Analysis of CPW for $LiNbO_3$ optical modulator by extended spectral-domain approach," *IEEE Microwave and Guided Wave Lett.*, vol. 2, no. 8, pp. 313–315, Aug. 1992.

[13] K. Kawano, T. Kitoh, H. Jumonji, T. Nozawa, M. Yanagibashi, and T. Suzuki, "Spectral-domain analysis of coplanar waveguide traveling-wave electrodes and their applications to Ti:$LiNbO_3$ Mach-Zehnder optical modulators," *IEEE Trans. Microwave Theory Tech.*, vol. MTT-39, no. 9, pp. 1595–1601, Sept. 1991.

[14] K. Kawano, K. Noguchi, T. Kitoh, and H. Miyazawa, "A finite element method(FEM) analysis of a shielded velocity-matched Ti:$LiNbO_3$ optical modulator," *IEEE Photon. Technol. Lett.*, vol. 3, no. 10, pp. 919–921, Oct. 1991.

[15] T. Kitazawa, D. Polifko, and H. Ogawa, "Simplified analysis of coplanar waveguide for $LiNbO_3$ optical modulator by variational method," *IEICE Trans. Electron.*, vol. E76-C, no. 2, pp. 244–250, Feb. 1993.

[16] T. Kitoh and K. Kawano, "Modeling and Design of Ti:$LiNbO_3$ optical modulator electrodes with a buffer layer," *IEICE Trans.*, vol. J75-C-I, no. 6, pp. 422–429, June 1992.

[17] T. Miyoshi, M. Sumiya, and H. Omori, "Analysis of an induction heating system by the finite element method combined with a boundary integral equation," *IEEE Trans. Magn.*, vol. MAG-23, pp. 1827–1832, Mar. 1987.

[18] T. Miyoshi and G. Maeda, "Finite element analysis of leakage Magnetic flux from an induction heating system," *IEEE Trans. Magn.*, vol. MAG-18, pp. 917–920, May 1982.

[19] X. Zhang and T. Miyoshi, "Influence of cross-sectional deformation on coplanar waveguide characteristics for the use of optical modulator," submitted to *IEICE Trans. Electron.*

[20] M. Abramowitz and I. A. Stegun, *Handbook of Mathematical Functions*, pp. 587–626, Dover, New York, 1972.

[21] R. C. Alferness, "Waveguide electrooptic modulator," *IEEE Trans. Microwave Theory Tech.*, vol. MTT-30, no. 8, pp. 1121–1137, Aug. 1982.

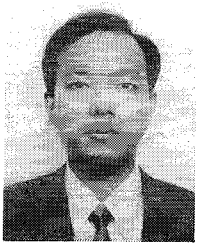

Xiang Zhang was born in Beijing, China, on February 6, 1963. He received the B.E. and M.E degrees in electronics engineering from Tsinghua University, Beijing, China, in 1985 and 1987, respectively. Since 1991, he has been working towards his Ph.D. degree in the Graduate School of Science and Technology, Kobe University, Japan.

From 1988 to 1990, he was with the Optical Fiber Laboratory at Shanghai Ceramics Institute, Academia Sinica. During that period, he engaged in research on bow-tie polarization-maintaining optical fiber, Er-doped single-mode optical fiber, and fiber thermo-sensors. His research interests include electro-magnetic field analysis for optical communication devices and process and measurement techniques for optical fibers.

Mr. Zhang is a menber of the Institute of Electronics, Information and Communication Engineers of Japan.

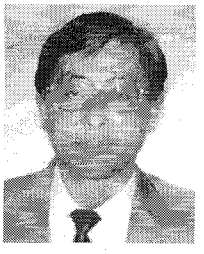

Tanroku Miyoshi (S'67–M'72) was born in Osaka, Japan, on January 6, 1944. He received the B.S., M.S., and Ph.D. degrees, all in electronic engineering, from the University of Tokyo, Tokyo, Japan, in 1967, 1969, and 1972, respectively.

In 1972 he was appointed lecturer, and from 1974 to 1987 he was an associate professor in the Department of Electronic Engineering, Kobe University, Kobe, Japan, where he is presently a professor. He has been engaged in research of electromagnetic wave theory, microwave integrated circuits, and lightwave electronics. His current research includes the quantum transport modeling in nanostructure devices, the electrical and optical characterization of heterojuctions, and the photonic integrated circuits. In 1976 he was a Visiting Scholar at McGill University, Montréal, Canada. From 1982 to 1984, he was a Visiting Scientist at Bell Laboratories, Holmdel, NJ USA.

Dr. Miyoshi is a member of the Institute of Electronics, Information and Communication Engineers of Japan and the Japan Society of Applied Physics. He received a Yonezawa Award in 1974 and an Outstanding Book Award in 1977, both from the Institute of Electronics, Information and Communication Engineers of Japan.